forests

Article

Continuous Leaf Area Index (LAI) Observation in Forests: Validation, Application, and Improvement of LAI-NOS

Zhentao Gao [1], Yunping Chen [1,*], Zhengjian Zhang [2], Tianxin Duan [1], Juncheng Chen [1] and Ainong Li [2]

[1] School of Automation Engineering, University of Electronic Science and Technology of China, No. 2006, Xiyuan Ave, West High-Tech Zone, Chengdu 611731, China; 202121060417@std.uestc.edu.cn (Z.G.); 202121060418@std.uestc.edu.cn (T.D.); 202122060139@std.uestc.edu.cn (J.C.)
[2] Institute of Mountain Hazards and Environment, Chinese Academy of Sciences, No. 9, Section 4, South Renmin Road, Chengdu 610041, China; zhangzj@imde.ac.cn (Z.Z.); ainongli@imde.ac.cn (A.L.)
* Correspondence: chenyp@uestc.edu.cn

Abstract: The leaf area index (LAI) is one of the core parameters reflecting the growth status of vegetation. The continuous long-term observation of the LAI is key when assessing the dynamic changes in the energy exchange of ecosystems and the vegetation's response indicators to climate change. The errors brought about by non-standard operations in manual LAI measurements hinder the further research utilization of this parameter. The long-term automatic LAI observation network is helpful in reducing errors from manual measurements. To further test the applicability of automatic LAI observation instruments in forest environments, this study carried out comparative validation research of the LAI-NOS (LAI automatic network observation system) at the Wanglang Mountain Ecological Remote Sensing Comprehensive Observation Station, China, comparing it with the results measured by the LAI-2200 Plant Canopy Analyzer (LI-COR, Lincoln, NE, USA), the LAI-probe handheld instrument, and a fisheye lens digital camera (DHP method). Instead of using the original "smoothest window" method, a new method, the "sunrise–sunset" method, is used to extract daily LAI-NOS LAI, and the corresponding confidence level is used to filter the data. The results of the data analysis indicate the following: LAI-NOS has a high data stability. The automatically acquired daily data between two consecutive days has a small deviation and significant correlations. Single-angle/multi-angle LAI measurement results of the LAI-NOS have good correlations with the LAI-2200 (R^2 = 0.512/R^2 = 0.652), the LAI-probe (R^2 = 0.692/R^2 = 0.619), and the DHP method (R^2 = 0.501/R^2 = 0.394). The daily LAI obtained from the improved method, when compared to the original method, both show the same vegetation growth trend. However, the improved method has a smaller dispersion. This study confirms the stability and accuracy of automatic observation instruments in mountainous forests, demonstrating the distinct advantages of automatic measurement instruments in the long-term ground observation of LAIs.

Keywords: leaf area index; hemispherical photography; LAI-NOS; LAI-2200

Citation: Gao, Z.; Chen, Y.; Zhang, Z.; Duan, T.; Chen, J.; Li, A. Continuous Leaf Area Index (LAI) Observation in Forests: Validation, Application, and Improvement of LAI-NOS. *Forests* **2024**, *15*, 868. https://doi.org/10.3390/f15050868

Academic Editor: Nikolay S. Strigul

Received: 26 April 2024
Accepted: 14 May 2024
Published: 16 May 2024

1. Introduction

A leaf area index (LAI) is defined as half of the leaf surface area per unit area and plays a critical role in ecological and agricultural research [1–3]. Long-term measurements of LAI are of great significance for studying climate change, ecosystems, and crop growth [4–8].

Satellite-based LAI products have played a crucial role in various fields, including land surface models. Remote sensing techniques enable the estimation of the LAI through empirical and model inversion methods using data from optical sensors, LiDAR, and microwave sensors. These methods rely on the relationship between vegetation reflectance or indices and the LAI, with adjustments for environmental and atmospheric conditions. Empirical approaches often use vegetation indices, while model inversion involves radiative transfer models. Both face challenges like atmospheric effects and the need for vegetation-specific models, with the aim of accurately measuring the LAI across different ecosystems [9–11]. Due to the difficulty in establishing a reasonable model to describe the radiation transfer process in the canopy, the uncertainty of the input parameters of the model and the obvious deviation of some vegetation types from the assumptions of remote sensing inversion, the uncertainty associated with determining the LAI through this method has to be of deep concern, and there is an urgent need to verify the accuracy of LAI values through continuous ground measurements [12].

Currently, on-site ground LAI measurements mainly rely on manual handheld instruments using indirect methods [13–15]. Commonly used measurement instruments include the LAI-2200 Plant Canopy Analyzer, AccuPAR, TRAC, CI-110, and other instruments, as well as the DHP method [12–14,16–18]. The principle of LAI measurements is based on the Beer–Lambert law [16], calculating light radiation attenuation or image gap fraction in order to obtain the LAI value [19,20]. Handheld measurements have high requirements for the operator's operational norms and suitable weather conditions under equal measurement conditions [21]. Moreover, an increasing number of experiments require long-term high-frequency ground observations of the LAI, making the deployment of LAI ground-based automatic observation instruments within the target study area highly practical [12,22,23].

Due to the significant advantages of automatic observation instruments, several LAI automatic observation technologies have been developed. For example, PASTIS-57 continuously monitors the LAI using a 57.5° zenith angle with a blue channel [18]. The LAINet is based on wireless sensor networks and automatically observes leaf area index (LAI) by measuring the downward solar radiation below the canopy at a central wavelength of 650 nm [23]. Comella et al. provided long-term automated monitoring data for both the LAI and PAR using a single microcontroller-based spectral sensor [24]. Kim et al. developed an integrated system 4S using a mini-computer, multispectral sensor, and RGB camera to sustainably monitor the NDVI, LAI, EVI, and fPAR [25]. Culvenor et al. developed a low-cost, automated, and semi-permanent ground-based LAI observation instrument IML using a laser rangefinder [26]. AHS automatically measured the plant area index (PAI) in forests by observing the direct radiation passing through the vegetation canopy and calculating the multi-angle scattered radiation transmission [27]. However, previous studies may not have paid much attention to the performance of these instruments when being used in forests in mountains.

East Asia forms a complex geomorphological structure, characterized by relatively steep slopes and rugged terrain, as compared to surrounding regions [28]. For forests in the mountain, the fine-scale topographical differences have a significant impact on its structure [29]. A complex three-dimensional structure of the forest can result in varying degrees of discrepancy in the footprint of a fisheye lens, according to the zenith and azimuth angles of the lens [30]. Considering these factors and the usability in both forests and crop fields, Chen et al. designed an LAI sensor based on the DHP method, and implemented the LAI-NOS automatic observation network system using a wireless sensor network [12]. The system has been applied and effectively validated in various research areas with different vegetation types in China. And the data of the LAI-NOS have been used to verify the MODIS LAI products [31]. Although the LAI-NOS has already been used on a larger scale, the further verification of the system's reliability in the mountainous forest and the performance in different weather conditions have not yet been fully tested. As the Wanglang National Nature Reserve, which is filled with mountainous forest resources and has a great need for automated LAI instruments, happen to be a new LAI-NOS deployment location, relevant experiments are necessary to be carried out.

This study aimed to conduct a comparative validation experiment between the LAI-NOS and the LAI-2200, LAI-probe, and manual camera DHP measurements, with the aim of providing a reference for the subsequent use of continuous LAI observation data in the Wanglang National Nature Reserve, and of exploring the data discrepancies in order to find the influencing factors when observing the LAI in mountainous forest areas using the LAI-NOS.

2. Materials and Methods

This study was undertaken to ascertain the reliability of the LAI-NOS in mountainous forests. Moreover, it aimed to compare the accuracy of three manual methods—LAI-2200, LAI-probe, and the DHP method—in similar environments. The research was conducted at the Wanglang Mountain Ecological Remote Sensing Comprehensive Observation Station, where 30 LAI-NOS nodes were set up across three distinct vegetation types. Data collection through the LAI-NOS spanned from 1 May 2023 to 10 July 2023. During this period, the LAI values were gathered using both multi-angle and single-angle approaches.

Additionally, on 29 May 2023 and 30 May 2023, the LAI values were measured at the 30 nodes using the LAI-2200, LAI-probe, and DHP method for comparative analysis.

2.1. Study Area and Data Acquisition

The research area is located in Pingwu County, Mianyang City, Sichuan Province, in the southwestern part of China. It is situated within the Wanglang National Nature Reserve, covering a total area of 322.97 km^2, with geographic coordinates ranging from 103°50′ to 104°58′ E and 32°49′ to 33°02′ N. The area lies at the northern edge of the Hengduan Mountains in the high-mountain canyon region, at the junction of the Qinghai-Tibet Plateau and the Sichuan Basin. The elevation gradually slopes from northwest to southeast, ranging from 2300 to 4980 m above sea level. The climate in the area exhibits a vertical distribution trend, characterized by warm, cold, subfrigid, and frozen zones as the altitude increases. The region experiences a typical Danba-Songpan semi-humid climate. Abundant water resources can be found in the reserve, with major tributaries including Changbaigou, Dawodang, and Zhugenchagou, which eventually flow into the upstream BaiMa River of the Fujiang River, thus forming the primary catchment area for the Fujiang River. The forested area within the reserve is approximately 169.40 km^2, accounting for 52.1% of the total area, and constituting the main part of the southwestern forest region, the second-largest forested area in China. The vertical vegetation spectrum consists of coniferous and broad-leaved mixed forests (2300–2600 m), *Abies fargesii* var. *faxoniana (Rehder & E. H. Wilson) Tang S. Liu* and *Picea purpurea Mast.* forests (2600–3500 m), subalpine shrub meadows (3500–4400 m), and alpine rock vegetation (4400–4900 m). The forest at the lower elevations (2700 m to 3200 m) mainly comprises *Abies faxoniana* and *Picea purpurea*. The sunny slopes consist of a mixed forest of *Abies faxoniana*, *Betula platyphylla Sukaczev*, *Betula albosinensis Burkill*, *Picea purpurea*, and *Juniperus squamata Buch.-Ham. ex D. Don*. On the rocky and ridge tops, with poor soil between 2700 m and 3200 m, *Juniperus squamata* is mainly found.

The Wanglang Mountain Ecological Remote Sensing Comprehensive Observation Station has three permanent observation sites, all representing different vegetation types (coniferous forest, mixed forest, and shrub forest) and altitudes. Each site has an observation tower with heights of 10 m, 30 m, and 75 m, respectively. The 10 m tower is located at 104.033° E, 33.005° N, mainly representing shrub forests. The 30 m tower is located at 104.055° E, 32.989° N, representing mixed forests. The 75 m tower is located at 104.016° E, 32.999° N, representing coniferous forests. Each observation tower is equipped with a set of LAI-NOS systems for long-term automatic LAI observations. Each system consists of 10 data collection nodes for measuring the LAI values in each site. It is particularly important to note that 10 m, 30 m, 75 m are just the names of the observation towers where the LAI-NOS's sink nodes are deployed nearby. So, the FOV of the cameras have nothing to do with the towers. The distribution of these nodes is shown in Figure 1, and the real scene of the sites is depicted in Figure 2.

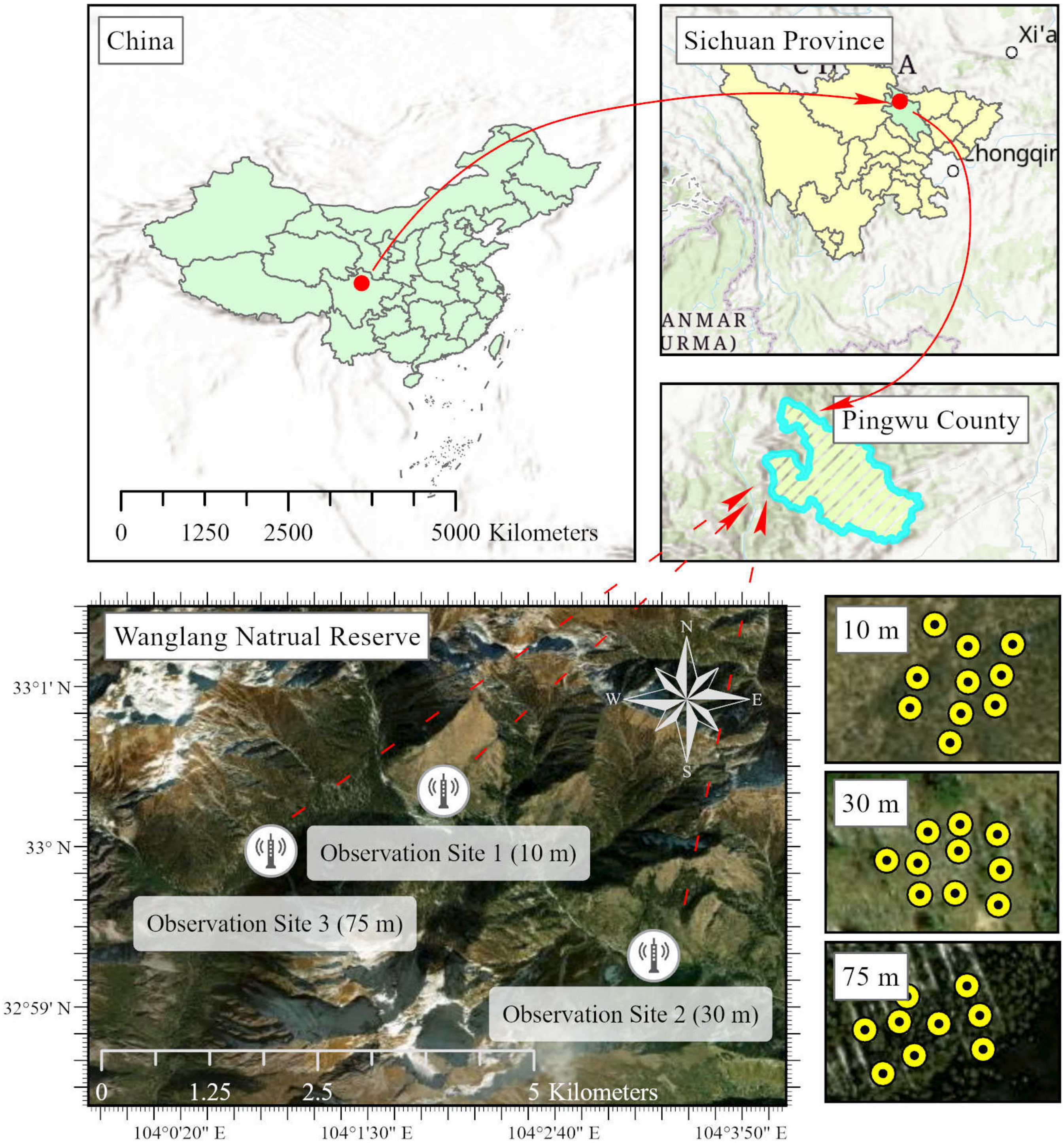

Figure 1. The research area located in the Wanglang National Nature Reserve, Pingwu County, Mianyang City, Sichuan Province, southwestern China. The first row of images shows the geographic location of the research area. The second row of images displays the distribution of the LAI-NOS nodes at three different locations with observation towers at heights of 10 m, 30 m, and 75 m.

Figure 2. Experimental area real scene. The first row of pictures are the real pictures of the 10 m tower, 30 m tower, and 75 m tower sample site. The pictures in the second row are the field drawings of the LAI-NOS nodes installed at the three sample sites. The three pictures in the third row from left to right are the field pictures of the manual measurements at the LAI-NOS nodes using the LAI-2200, LAI-probe, and digital cameras with fisheye lenses.

The LAI values were measured using the LAI-2200 canopy analyzer and the LAI-probe at the LAI sensor locations of each LAI-NOS system. And a fisheye digital camera (Canon EOS 600D camera (Canon, Tokyo, Japan) + Canon EF 8–15 mm f/4L USM fisheye lens) was used to capture the DHP images (as shown in Figure 2). In order to reduce the influence of the manual measurement operations on the results, the measurements were repeated for each LAI-NOS node multiple times (in which, the LAI-2200 was measured twice and the LAI-probe and DHP were measured three times), and the average value was taken as the measurement result. Due to the dense forest in the experimental area, the LAI-2200 double-probe method was adopted for measurement. The 75 m and 10 m sites were measured on 29 May 2023, with the weather ranging from cloudy to overcast. The 30 m sample was measured on 30 May 2023, with the weather ranging between cloudy and light rain. Figure 3 shows two examples of thumbnail images taken by the LAI-NOS nodes on that day.

Figure 3. Example of the thumbnail sent back by the LAI-NOS.

2.2. Experimental Equipment

Table 1 lists the relevant parameters of the LAI-NOS and the experimental equipment used in the three manual measurement methods. Since all of the experimental equipment adopted the optical method for the LAI numerical calculation, all branches, trunks, fruits, flowers, and other light barriers within the field of view of the LAI-NOS nodes in the sample site were included in the leaf area index. And the measurement result was actually the plant area index (PAI) [32]. The PAI, when measured using indirect methods, usually includes the area of the woody part, as well as the area of unhealthy leaves. The area of the wooden part, the woody area index (WAI), is often difficult to estimate efficiently and conveniently using the indirect method [33]; for the upward method, it is also difficult to efficiently separate the healthy leaf part [34]. In order to simplify the analysis process, the LAI was used in this study, and the concepts of the PAI, LAI, or green area index (GAI) were no longer separately distinguished [35].

Table 1. Parameters of the experimental instruments used for measurement.

Instrument	Channel	Sampling Angle	Orientation	Measuring Height
LAI-2200	Blue	0.0–12.3°; 16.7–28.6°; 32.4–43.4°; 47.3–58.1°; 62.3–74.1°.	Upward	50 cm above ground
LAI-NOS	Blue	55°–60°; 0.0–12.3°; 16.7–28.6°; 32.4–43.4°; 47.3–58.1°; 62.3–74.1°.	Upward	50 cm above ground
LAI-probe	Blue	55°–60°.	Upward	50 cm above ground
DHP	Blue	55°–60°.	Upward	50 cm above ground

2.2.1. LAI-2200 Plant Canopy Analyzer

The LAI-2200 Plant Canopy Analyzer, designed and manufactured by LI-COR Inc. (Lincoln, NE, USA), features a unique fisheye optical sensor with a 148° field of view. It measures the interception of blue light from five different zenith angles and uses a radiation transfer model to calculate the leaf area index (LAI) of the canopy. The study's three sample sites are located in mountainous forests with tall and dense vegetation canopies, making it challenging to use the single-probe method for LAI measurements with the LAI-2200. To overcome this challenge, the study used the LAI-2200 in a double-probe method for LAI measurements. One probe was set in an automatic timed sampling mode, measuring A values every 30 s. Simultaneously, another probe was used to take two repeated measurements of B values at the LAI-NOS sensor bracket at each node. "A values" represent LAI-2200 readings in an open field (above canopy), while "B values" are readings taken under the canopy. To ensure consistency with the sampling range of the fisheye photography method, no angle cover caps were used at any of the nodes during the LAI-2200 measurements.

After the field measurements were completed, the A and B values obtained using the double-probe method from the LAI-2200 were exported. The accompanying data processing software FV2200 (Version 2.1) was used to batch process the A and B values and calculate the LAI values for all nodes based on the double-probe measurements taken at each node.

2.2.2. LAI-Probe

The LAI-probe is a portable LAI measurement device based on fisheye photography technology [36]. The upgraded version of the LAI-probe used in this experiment has a polarizer added to the original lens, which significantly reduces the influence of internal reflection and scattering in the canopy. This improvement enhances the accuracy of canopy image segmentation and improves the measurement precision. The LAI-probe can measure various parameters, including the average leaf inclination angle, leaf area index (LAI), clumping index, and gap fraction. The LAI-probe handheld device consists of a fisheye lens, a rugged tablet, and a handheld bracket. It has a field of view angle of 210°, and its focal length is 1.05 mm. The JPEG format images captured by the LAI-probe has a resolution of 3200 × 2400. At each node, measurements were repeated three times (as shown in the middle image of the third row in Figure 2). The LAI calculation process with the LAI-probe is as follows: Firstly, a circular mask is used to extract the field of view angle of 180° from the image. Then, the foreground and background pixel numbers are counted and the gap fraction is calculated for the range of zenith angles between 55° and 60°. Finally, the effective LAI (LAI_{eff}) is calculated using Equation (1) as follows:

$$LAI_{eff} = -\frac{\ln P(\theta)\cos(\theta)}{G(\theta)} \tag{1}$$

where $G(\theta) \approx 0.5$, and $P(\theta)$ represents the gap fraction within the range of zenith angles between 55°and 60°.

2.2.3. LAI-NOS

The LAI-NOS consists of two main components as follows: the hardware deployed in the measurement area and the software on the server side, which is responsible for data reception, processing, querying, and measurement frequency control.

The system architecture (Figure 4) includes a sensor node, sink node, LAI sensor, server, and client. The LAI sensors capture the DHP images at regular intervals and perform the real-time calculations of canopy parameters, such as the leaf area index, clumping index, and mean leaf inclination angle. The data communication with the sensor nodes is facilitated through RS485. The LAI sensor, with an effective range of 0 to 12 m^2/m^2 and a resolution of 0.01 m^2/m^2, incorporates features like automatic exposure control, automatic gain control, automatic white balance, and automatic black level calibration. These functionalities ensure stable operation, high precision, and swift mass sampling, thus enhancing overall system performance. The computed data are then transmitted back to the data server through the sensor nodes and sink nodes. The data reception and processing program deployed on the server stores all raw data and, at the end of each day, automatically applies the daily LAI data extraction method to calculate the daily LAI values. For specific equipment information, refer to [12]. This system has been improved from its predecessor. Each LAI sensor now has the capability to periodically transmit canopy thumbnail images, thus facilitating the inspection of the lens cleanliness status.

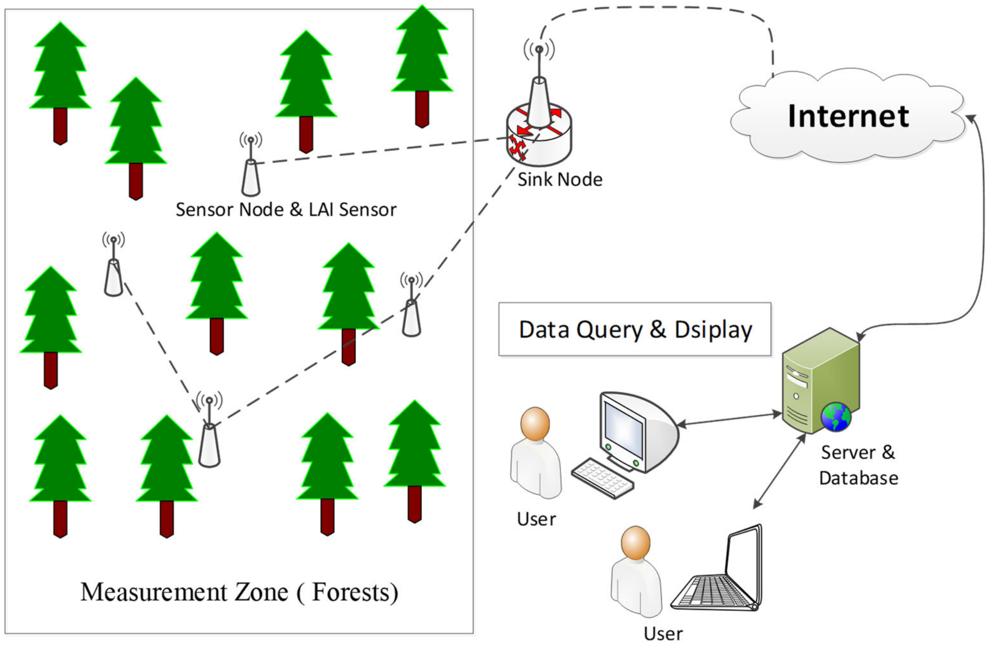

Figure 4. Overall system architecture diagram.

In April 2023, the Wanglang Mountain Ecological Remote Sensing Comprehensive Observation Station deployed a set of LAI-NOS systems at each of the three permanent observation sites, each consisting of 10 LAI measurement nodes, totaling 30 nodes. After installation and debugging, the LAI-NOS system began measuring and transmitting data at a frequency of once every 5 min. The deployed LAI-NOS devices can simultaneously calculate the LAI values using both the single-angle method and the multi-angle method. For the single-angle method, the LAI is determined using the DHP image zenith angle range between 55° and 60°, and the calculation equation is shown in Equation (1). For the multi-angle method, five zenith angle ranges (7°, 23°, 38°, 53°, 68°) are used, similar to the LAI-2200, in order to determine the LAI values, and the calculation equation is shown in Equation (2). The result is denoted as MLAI.

$$\mathrm{LAI_{eff}} = -2\int_0^{\frac{\pi}{2}} \ln P(\theta)\cos\theta\sin\theta d\theta \quad (2)$$

2.2.4. DHP

Using a fisheye camera (Canon EOS 600D camera + Canon EF 8–15 mm f/4L USM fisheye lens), hemispherical canopy images were obtained. The camera was placed at the same position as the LAI-NOS system's LAI sensor mount (height 0.5 m) to capture the canopy images (see Figure 2, third row, third image). In order to compare with the data obtained using the LAI-NOS automatic capture mode, three photos were taken using the camera's automatic exposure mode, with an image resolution of 5184 × 3456, and were saved in JPEG format. All the acquired DHP images were processed using the same platform as the LAI-probe with a single-angle method for calculating the LAI.

2.3. MODIS Data Acquisition

To compare with the LAI data obtained from ground instruments, the MODIS LAI product for the study area was processed using NASA's Land Processes Distributed Active Archive Center (LP DAAC) AppEEARS (Application for Extracting and Exploring Analysis Ready Samples) tool. We utilized AppEEARS to download all MCD15A3H LAI data with a quality flag FparLai_QC of 0 (indicating the best quality) for the three selected sites within the study area for the months from April to June 2023. Specifically, the LAI data for 11 April and 27 April 2023 were obtained for all three sites. Because the MODIS data are filtered using the quality flag, the MODIS LAI data do not exactly coincide with the LAI-NOS's data. The average LAI value for each site was calculated based on the data from the two days, and it will be used to compare the LAI trends of these three sites with other measurement methods.

2.4. Methodology

Validate the LAI-NOS comprised three steps (shown in Figure 5). The first step involved data collection using three kinds of handhold instruments. And the second step is extracting daily LAI data from continuous LAI-NOS data using the "sunrise–sunset" method and filtering the data using the confidence level. In the third step, data obtained from three handhold instruments are used to compare with the LAI-NOS daily LAI via the use of error analysis and regression analysis.

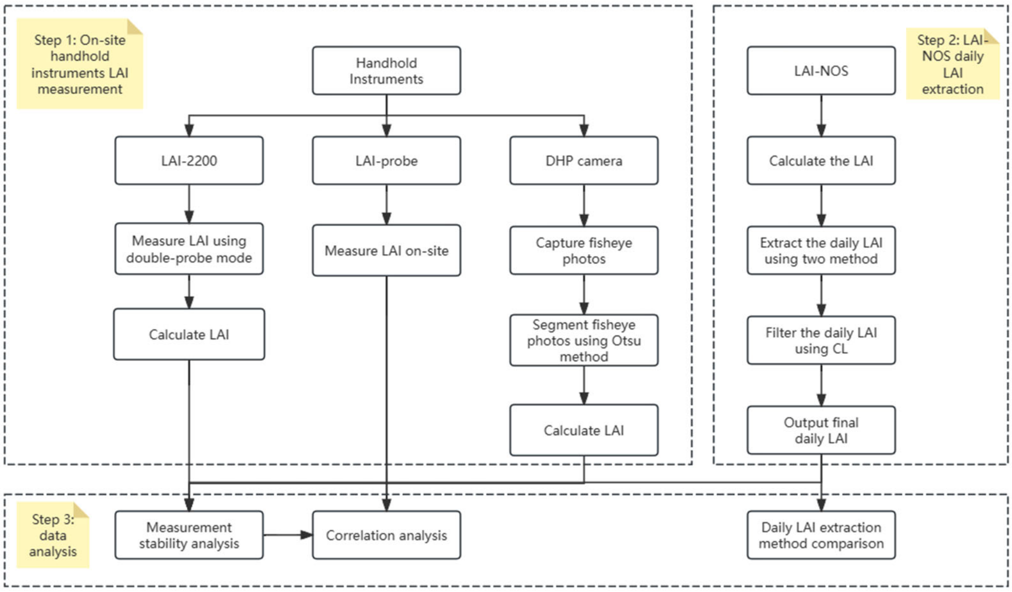

Figure 5. Flowchart of the study methodology.

2.4.1. LAI-NOS Daily LAI Data Extraction Method

The vegetation leaf area does not change much in the short term, and the difference in the continuous measurement results within one day should be small. However, being affected by changes in the light conditions, the LAI values obtained through continuous measurements will change significantly. In order to obtain the measurement results that can best represent the LAI of the measured sample site on the same day, the LAI-NOS developed the "smoothest window" method. This method effectively avoided the large error introduced by using the all-day average value, and effectively guaranteed the accuracy of the extracted daily LAI [12]. However, the "smoothest window" may appear at any time, especially in dense forest land. Due to the influence of complex light under the forest during the day, LAI values extracted using the "smoothest window" method are often too small.

Considering that scattered light conditions before sunrise, after sunset, and on cloudy days are the best light conditions for LAI optical measurements, this paper proposes the use of the "sunrise–sunset" method to extract daily LAI data. The specific practices are as follows: The exact time of the local sunrise and sunset is calculated based on node coordinates. And the instantaneous measurement results within 10 min before sunrise and 10 min after sunset are selected to calculate the average value, which are the sunrise LAI value LAI_{rise} and the sunset LAI value LAI_{set}. Then, the LAI of the day $LAI = (LAI_{rise} + LAI_{set})/2$.

2.4.2. LAI-NOS Daily LAI Data Filter Method

Assuming that the LAI value sees no significant change in one day, $LAI_{rise} \approx LAI_{set}$ should be assumed. But, in certain situations, such as the influence of dew or rainfall, significant differences between the LAI_{rise} and LAI_{set} may occur, making it difficult to rely on their average as the LAI value for that day. Based on this idea, we constructed the LAI confidence equation of the same day as follows:

$$CL = 1 - \frac{|LAI_{rise} - LAI_{set}|}{LAI_{rise} + LAI_{set}} \tag{3}$$

In Equation (3), CL represents confidence. Preliminary experiments show that, if CL < 0.5, as affected by weather and other factors, the LAI of the corresponding day is less reliable and the data quality is poor. So, it is not recommended to adopt it. If CL > 0.8, the LAI on the same day has a high reliability. If the data quality requirements are very high, CL can also be set as 0.9 or above.

After filtering the data with a confidence level greater than 0.8, the average absolute relative errors for the LAI-NOS automatic measurements at the 10 m, 30 m, and 75 m sites were 12.55%, 10.76%, and 10.25%, respectively, for the LAI, and 7.31%, 8.51%, and 8.04%, respectively, for the MLAI. When filtering the data with a confidence level greater than 0.9, the average absolute relative errors for LAI-NOS automatic measurements at the 10 m, 30 m, and 75 m sites were 12.07%, 10.38%, and 10.42%, respectively, for the LAI, and 7.26%, 8.69%, and 8.11%, respectively, for the MLAI.

2.5. Evaluation Criteria

We used the absolute error and relative error to measure the relative error between multiple measurements at the same site after completing the measurements to test the stability of all instruments.

Absolute error = First measurement − Second or third measurement.

Relative error = Absolute error/First measurement.

For the LAI and MLAI data, measured using the LAI-NOS, this study used 10 node measurements at each site to calculate the absolute error and relative error for the two adjacent days, taking the mean value as the average value for that site to measure the stability of the measurements at one site. Here, the absolute error and relative error are calculated as follows:

Absolute error = Measurement value on the first day − Measurement value on the second day.

Relative error = Absolute error/Measurement value on the first day.

And the *RMSE*, R^2, and *RRMSE* [37] are used to compare the LAI, as measured using the LAI-NOS and handhold instruments.

$$RMSE = \sqrt{\frac{1}{n}\sum_{i=1}^{n}\left(y_i^s - y_i^m\right)^2} \tag{4}$$

$$R^2 = 1 - \frac{\sum_{i=1}^{n}\left(y_i^s - y_i^m\right)^2}{\sum_{i=1}^{n}\left(y_i^s - \overline{y}^s\right)^2} \tag{5}$$

$$RRMSE = \left(\frac{RMSE}{\frac{1}{n}\sum_{i=1}^{n} y_i^m}\right) \times 100 \tag{6}$$

where n represents the size of the test samples; y_i^m denotes the LAI value measured at the i-th sensor node; and y_i^s represents the reference LAI value measured at the i-th sensor node. The higher values of the coefficient of determination R^2 suggest a better performance of the considered model. On the other hand, a lower value of *RMSE* or *RRMSE* is desirable, as it indicates better accuracy in the LAI measurement.

3. Results

3.1. Measurement Stability Analysis

To analyze the stability of the manual measurement methods, relative errors for multiple measurements using the LAI-2200, LAI-probe, and DHP methods were calculated, as shown in Figure 6.

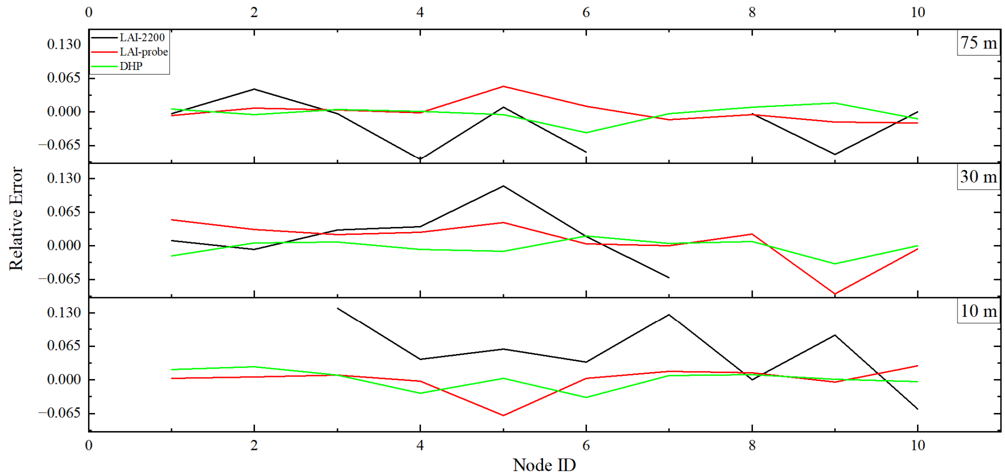

Figure 6. Relative error of manual repeated measurement results.

Figure 6 shows the average relative errors between multiple measurements of the LAI-2200, LAI-probe, and DHP methods at each sample site. At the 10 m tower site, the mean absolute relative error for the LAI-2200 measurements (two repetitions) is 7.31%, for the LAI-probe measurements (three repetitions), this is 1.52%, and for the DHP method measurements (three repetitions), this is 1.39%. At the 30 m tower site, the mean absolute relative error for the LAI-2200 measurements (two repetitions) is 5.71%, for the LAI-probe measurements (three repetitions), this is 3.01%, and for the DHP method measurements (three repetitions), this is 1.16%. At the 75 m tower site, the mean absolute relative error for the LAI-2200 measurements (two repetitions) is 13.15%, for the LAI-probe measurements (three repetitions), this is 1.41%, and for the DHP method measurements (three repetitions), this is 1.06%.

The regression analysis of the multiple measurements for each method yields the following determination coefficients: for LAI-2200 (two repetitions), the coefficient is 0.73 ($p < 0.05$); for the LAI-probe (three repetitions), the coefficients are 0.97 ($p < 0.05$), 0.97 ($p < 0.05$), and 0.99 ($p < 0.05$); and for the DHP method (three repetitions), the coefficients are 0.99 ($p < 0.05$), 0.99 ($p < 0.05$), and 0.99 ($p < 0.05$). All three methods show significant correlations between the results obtained from multiple repetitions.

In continuous two-day periods, LAI values should exhibit no significant changes, indicating that measurements at the same location should remain stable. The data of day 1 and day 2 are used to validate the stability of the LAI-NOS. We regard both measurements of day 1 and day 2 as correct values. Due to the minor changes of the leaf area across two consecutive days, the error can reflect the degree of stability. To analyze the stability of the instrument, we assessed the relative errors of the LAI-NOS measurements for the adjacent two-day periods. The specific procedure involved calculating the relative error for each node's measurement data from 1 May to 10 July. The average relative error for the ten nodes' positions was considered the instrument's relative error for that specific site. Based on this analysis, the system's relative errors for the measurement period at each site were obtained, as depicted in Figures 7–9.

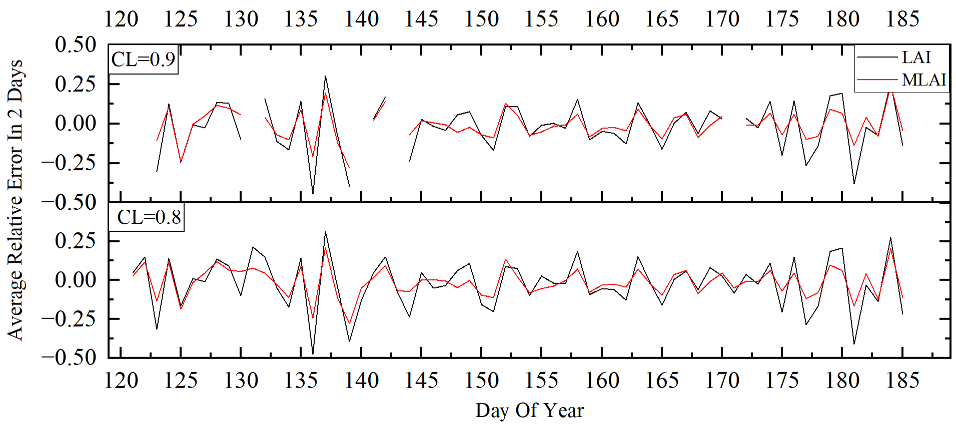

Figure 7. The average LAI relative error of two adjacent days from 1 May to 10 July (10 m).

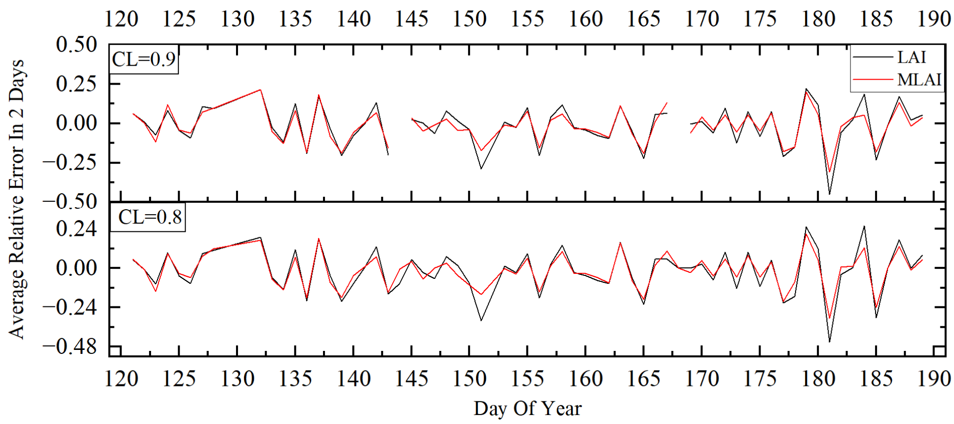

Figure 8. The average LAI relative error of two adjacent days from 1 May to 10 July (30 m).

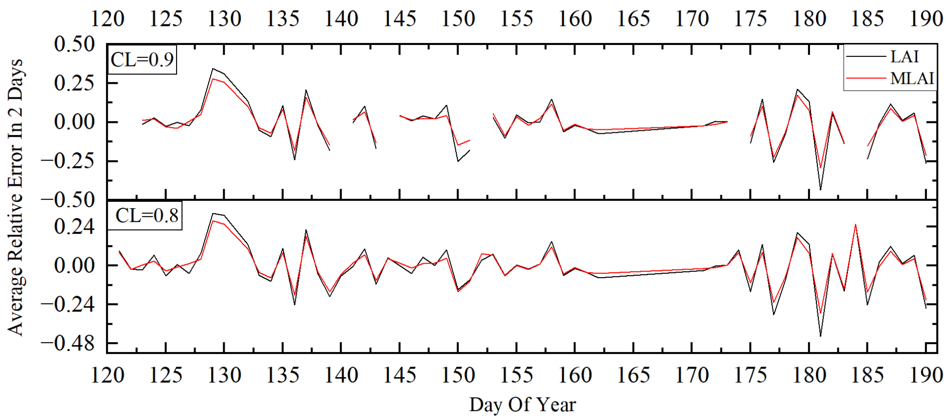

Figure 9. The average LAI relative error of two adjacent days from 1 May to 10 July (75 m).

From the results of the adjacent day measurements, it can be observed that, regardless of whether a confidence level of 0.9 or 0.8 is used for data filtering, the MLAI data has lower relative errors than the LAI data. The percentage of days with relative errors below 20% for the LAI at the three sites is greater than 80%, while, for the MLAI, it is greater than 90%.

Since the 10 nodes are distributed at different locations within the experimental site, the consecutive two-day measurements at these nodes should exhibit good correlation. The analysis of the correlation between the adjacent day measurements from the LAI-NOS is shown in Figure 10.

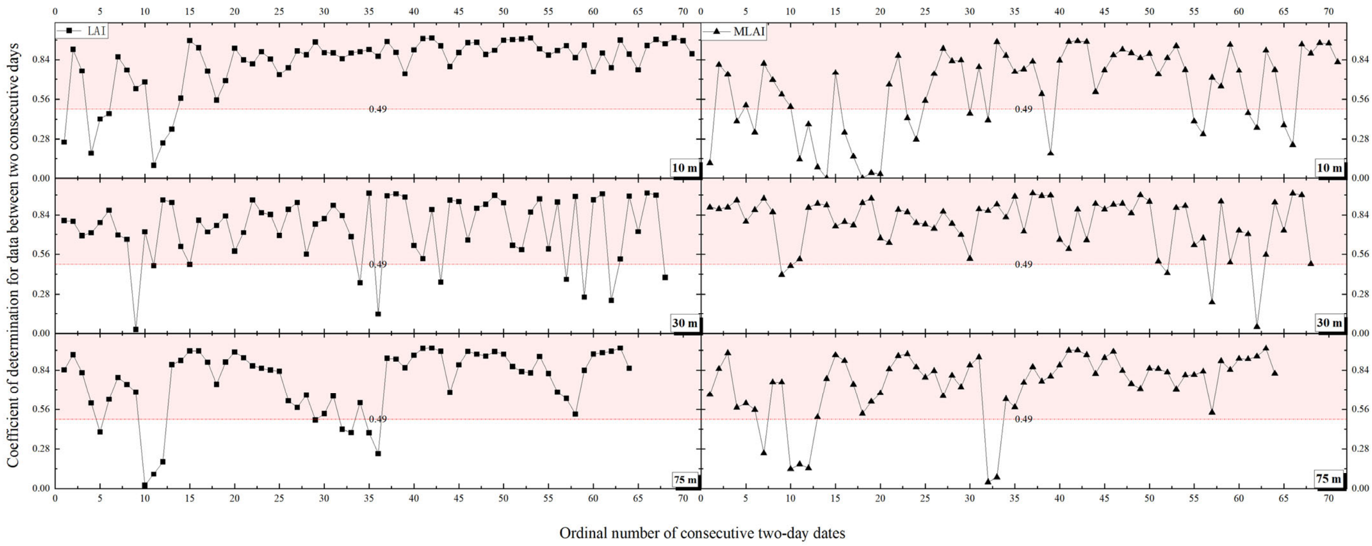

Figure 10. Correlation coefficient of the LAI-NOS data of two consecutive days. The left side lists the two-day correlation of the LAI data, and the right side lists the two-day correlation of the MLAI data. From the first row to the third row, the sites are 10 m, 30 m, and 75 m.

During the measurement period, there were no significant changes in vegetation and no human disturbances, such as logging. Therefore, it can be assumed that the average LAI values remained constant between the adjacent days, and there was a correlation between the measurements at each node on adjacent days. From Figure 10, it can be seen that, during the study period, most of the adjacent day LAI data showed a significant correlation (determination coefficient greater than 0.49, as indicated by the light red area in the graph) [38].

In summary, the LAI-NOS LAI/MLAI values between the adjacent days at the 30 m, 10 m, and 75 m sites showed significant correlation, with similar values on adjacent days, indicating stable measurement results.

The average LAI values of the different measurement methods at the three sites are as shown in Figure 11:

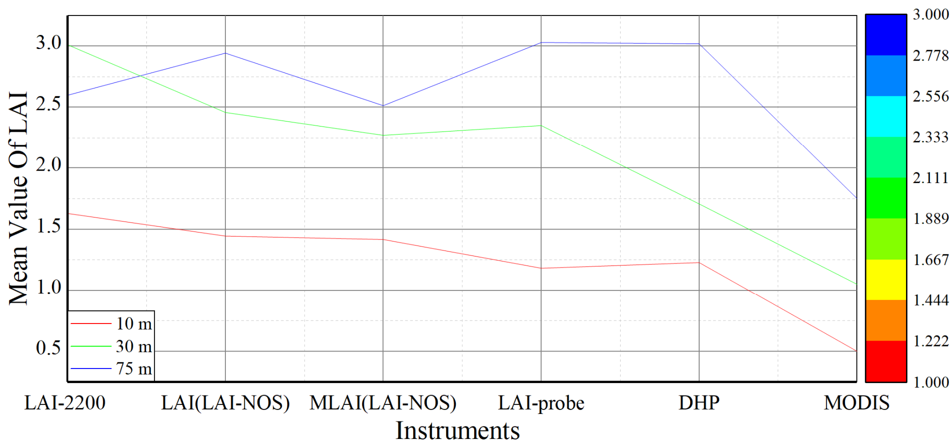

Figure 11. Average values of the measurement results of the different methods at three sites.

On 29 May, manual LAI measurements were conducted at 10 m and 75 m sampling sites, while the LAI-NOS data were taken on the same day. The average LAI-2200 measurement at the 10 m site was 1.54, while the LAI-NOS values were recorded as 1.44/1.42 (LAI/MLAI).

At the 75 m sampling site, the LAI-NOS system recorded values within a range of 2.28~3.35/2.18~2.7 (LAI/MLAI), with an average value of 2.94/2.51(LAI/MLAI). The LAI-2200 measurements for the same site ranged from 0.97~3.38, with an average value of 2.60.

On 30 May, a manual LAI measurement was carried out at the 30 m sampling site, and the LAI-NOS data were taken on the same day. The LAI-NOS system recorded values within a reasonable range of 1.91~3.2/1.91~2.87(LAI/MLAI), with an average value of 2.46/2.27(LAI/MLAI). The LAI-2200 measurements for the same site ranged from 1.30~4.88, with an average value of 3.01.

Table 2 shows what percentage of the MODIS LAI is underestimated for three sites.

Table 2. Underestimated value (%) of MODIS LAI.

	LAI-2200	LAI-NOS LAI	LAI-NOS MLAI	LAI-Probe	DHP
10 m	47.7887	41.09494	39.97175	27.9661	30.78176
30 m	53.51926	43.01994	38.35315	40.42553	17.93669
75 m	11.50442	21.82189	8.512331	24.09241	23.81583

3.2. Analysis Correlation

Due to the limitation of the number of permitted installments, we have only 30 sets of LAI sensor nodes deployed in the research area. For comparison with the LAI-2200, we removed the data collected from two points, where the LAI-2200 has a blank outcome. The linear regression analysis was performed on the data obtained from 28 points using the LAI-2200, LAI-probe, and fisheye camera DHP method, comparing them with the LAI-NOS LAI and MLAI measurements. Two points with LAI-2200 measurements equal to 0 were excluded from the analysis. The results are shown in Figure 12:

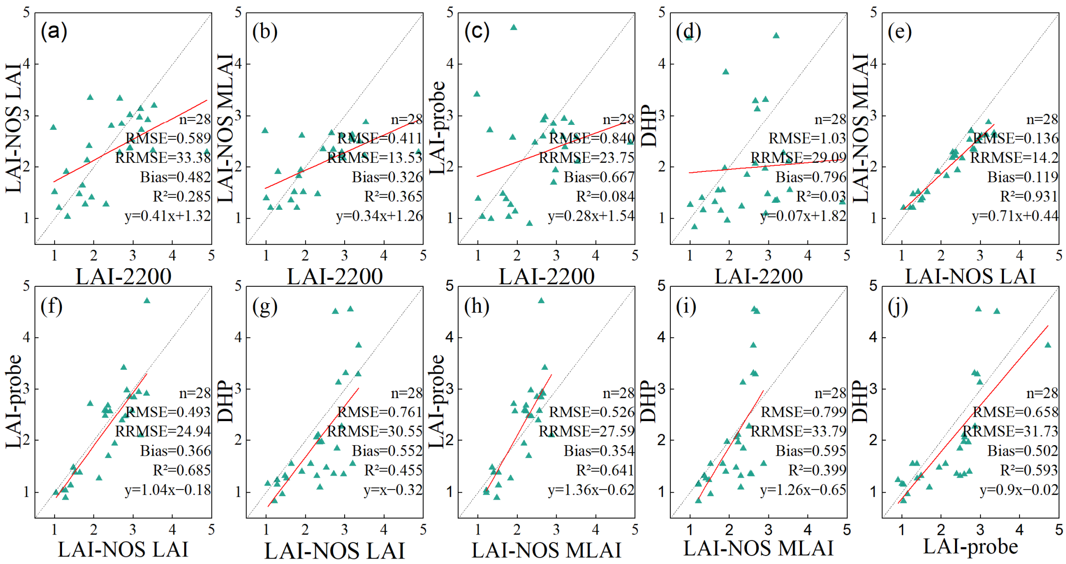

Figure 12. Correlation analysis among the measurement methods. (**a**) regression analysis between measurements of LAI-NOS LAI and LAI-2200; (**b**) regression analysis between measurements of LAI-NOS MLAI and LAI-2200; (**c**) regression analysis between measurements of LAI-probe and LAI-2200; (**d**) regression analysis between measurements of DHP and LAI-2200; (**e**) regression analysis between measurements of LAI-NOS MLAI and LAI-NOS LAI; (**f**) regression analysis between measurements of LAI-probe and LAI-NOS LAI; (**g**) regression analysis between measurements of DHP and LAI-NOS LAI; (**h**) regression analysis between measurements of LAI-probe and LAI-NOS MLAI; (**i**) regression analysis between measurements of DHP and LAI-NOS MLAI; (**j**) regression analysis between measurements of DHP and LAI-probe.

The regression analysis results indicate the following correlations between the LAI-NOS measurements and the other measurement methods: (1) LAI-NOS LAI vs. LAI-2200: The determination coefficient is 0.285, and the p-value is 3.417×10^{-3} demonstrating that there is a significant correlation between the LAI-NOS LAI and LAI-2200. The correlation is relatively weak. (2) LAI-NOS MLAI vs. LAI-2200: The determination coefficient is 0.365, and the p-value is 6.64×10^{-3}, indicating a significant correlation between the LAI-NOS MLAI and LAI-2200. The correlation is relatively weak. (3) LAI-NOS LAI vs. LAI-probe: The determination coefficient is 0.685, and the p-value is 5.55×10^{-8}, demonstrating a highly significant correlation between the LAI-NOS LAI and LAI-probe. The correlation is strong. (4) LAI-NOS MLAI vs. LAI-probe: The determination coefficient is 0.641, and the p-value is 3.16×10^{-7}, indicating a highly significant correlation between the LAI-NOS MLAI and LAI-probe. The correlation is relatively strong. (5) LAI-NOS LAI vs. fisheye camera DHP method: The determination coefficient is 0.455, and the p-value is 8.3×10^{-5}, showing a significant correlation between the LAI-NOS LAI and the fisheye camera DHP method. The correlation is relatively strong. (6) LAI-NOS MLAI vs. fisheye camera DHP method: The determination coefficient is 0.399, and the p-value is 3.11×10^{-4}, indicating a significant correlation between the LAI-NOS MLAI and the fisheye camera DHP method. The correlation is relatively strong.

The RRMSE is calculated using the LAI marked below the x-axis as y_i^s, and the LAI marked near the y-axis as y_i^m. In Figure 12, it is clear that, whether we use the LAI-2200 or LAI-NOS LAI as the reference LAI, the LAI-NOS MLAI shows smallest RRMSE, which indicates that the LAI-NOS MLAI has the best measurement accuracy.

Overall, the regression analysis confirms that there is a significant and relatively strong correlation between the LAI-NOS measurements and the measurements obtained from the LAI-probe and the fisheye camera DHP method, and a significant and weak correlation between the LAI-NOS measurements and the measurements obtained from the LAI-2200. The results suggest that the LAI-NOS is a reliable and relatively accurate alternative to traditional manual measurement methods for obtaining LAI data.

Due to the influence of factors such as the operation mode, measurement position, and weather conditions in the measurement process of manual measuring instruments, some outliers with obvious differences from other measurement results will appear in the results. After eliminating the two significant deviations in manual measurement results, the regression analysis is performed again, indicating the following: The coefficient of determination between the LAI data obtained using the LAI-NOS and LAI-2200 increased to 0.512, showing a significant correlation. The coefficient of determination between the MLAI data obtained using the LAI-NOS and LAI-2200 was 0.652, indicating a significant correlation. The determination coefficient between the LAI data obtained using the LAI-NOS and LAI-probe was 0.692, indicating a significant correlation. The determination coefficient between the MLAI data obtained using the LAI-NOS and LAI-probe was 0.619, showing a strong correlation. The coefficient of determination between the LAI data obtained using the LAI-NOS and DHP method of the fisheye camera was 0.501. The coefficient of determination between the MLAI data obtained using the LAI-NOS and the fisheye camera DHP method was 0.394. Among the manual measuring instruments, the coefficients of determination between the LAI-2200 and LAI-probe and the fisheye camera DHP method were 0.189 and 0.132, respectively, which showed that the correlation was still poor. The coefficient of determination between the LAI-probe and the fisheye camera DHP method was 0.600, indicating a good correlation.

In general, there was a strong correlation between the LAI-NOS and LAI-2200 and the LAI-probe and DHP measurement data of the fisheye camera at the three sites, indicating that the automatic instrument was in good agreement with the manual measurement method. After the obvious outliers caused by manual operation and weather change were removed, the LAI-NOS was significantly correlated with the manual measurement results. Among the manual measurements, there was a significant correlation between the LAI-probe and the fisheye camera DHP method, but a poor correlation between the LAI-2200 and LAI-probe, indicating that there were two different trends in the measurement results of the three manual measurement methods in the study area.

3.3. Comparison of LAI-NOS Daily LAI Data Extraction Methods

Figure 13 shows the results of the daily LAI data obtained by the two nodes using the "smoothest window" method and the "sunrise–sunset" method, respectively (raw data, data filtered by CL = 0.8 and data filtered by CL = 0.9). The measurements were taken from 9 May to 13 June 2023.

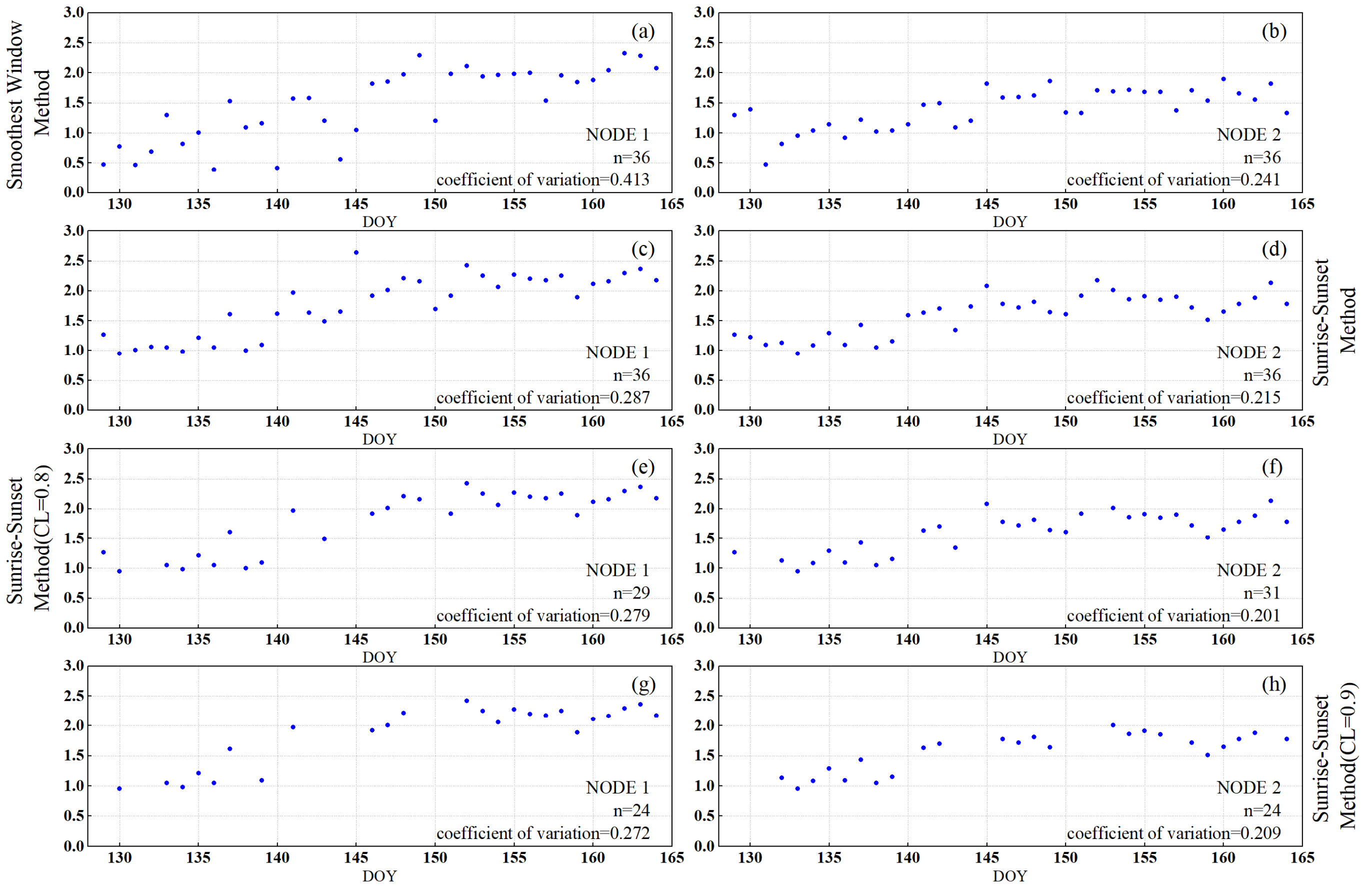

Figure 13. Comparison of the daily LAI data extraction methods. Scatter plots of the daily LAI results using the "smoothest window" method for Node 1 and Node 2 during the study period are shown in (**a**,**b**), respectively. Scatter plots of the daily LAI results using the "sunrise–sunset" method for Node 1 and Node 2 during the study period are shown in (**c**,**d**), respectively. Scatter plots of the daily LAI results using the "sunrise–sunset" method with filtering CL = 0.8 for Node 1 and Node 2 during the study period are shown in (**e**,**f**), respectively. Scatter plots of the daily LAI results using the "sunrise–sunset" method with filtering CL = 0.9 for Node 1 and Node 2 during the study period are shown in (**g**,**h**), respectively.

From Figure 13, it is evident that both the "smoothest window" method and the "sunrise–sunset" method yield LAI daily data with a clear increasing trend as the day of year (DOY) increases. However, when compared to the "smoothest window" method, the newly introduced "sunrise–sunset" method in this study can achieve lower coefficients of variation and reduced variability, which means that the "sunrise–sunset" method is a better choice. After applying confidence filtering to the data, the "sunrise–sunset" method produces a LAI time series with even lower coefficients of variation. Selecting a confidence level of 0.9 for data filtering results in only a small difference in the coefficients of variation when compared to using a confidence level of 0.8. This indicates that a confidence level of 0.8 is sufficient to obtain high-quality daily LAI data without significantly reducing the number of valid data points due to overly stringent filtering conditions.

3.4. LAI-NOS Time Series of Measurement Results

The LAI-NOS automatic observation system continuously observes the canopy at the node and is very sensitive to the dynamic change of leaf area index. The LAI-NOS automatic observation system of Wanglang Mountain Ecological Remote Sensing Comprehensive Observation Test Station was installed on 26 April 2023, and has begun continuous observation after debugging. Taking the daily data from 1 May 2023 to 10 July 2023 (the data of 30 m tower sites and 75 m tower sites had lost days) as an example, the temporal changes of LAI during the vegetation growing season in the three sites were analyzed.

As shown in Figures 14 and 15, it can be observed that the LAI and MLAI measured by the LAI-NOS automatic observation system at the three sites all show an increasing trend from 1 May to 10 July. This period coincides with the vegetation germination and leaf growth phase in the experimental area, which is consistent with the actual situation. Among them, the 10 m and 30 m sites exhibit a more pronounced upward trend in measurements, while the 75 m site shows a relatively gradual increase. This is mainly because the 75 m site is dominated by evergreen coniferous forests, which have relatively small changes in leaf area index, while the 10 m and 30 m sites are dominated by deciduous broadleaf forests, which experience rapid growth and significant changes in leaf area.

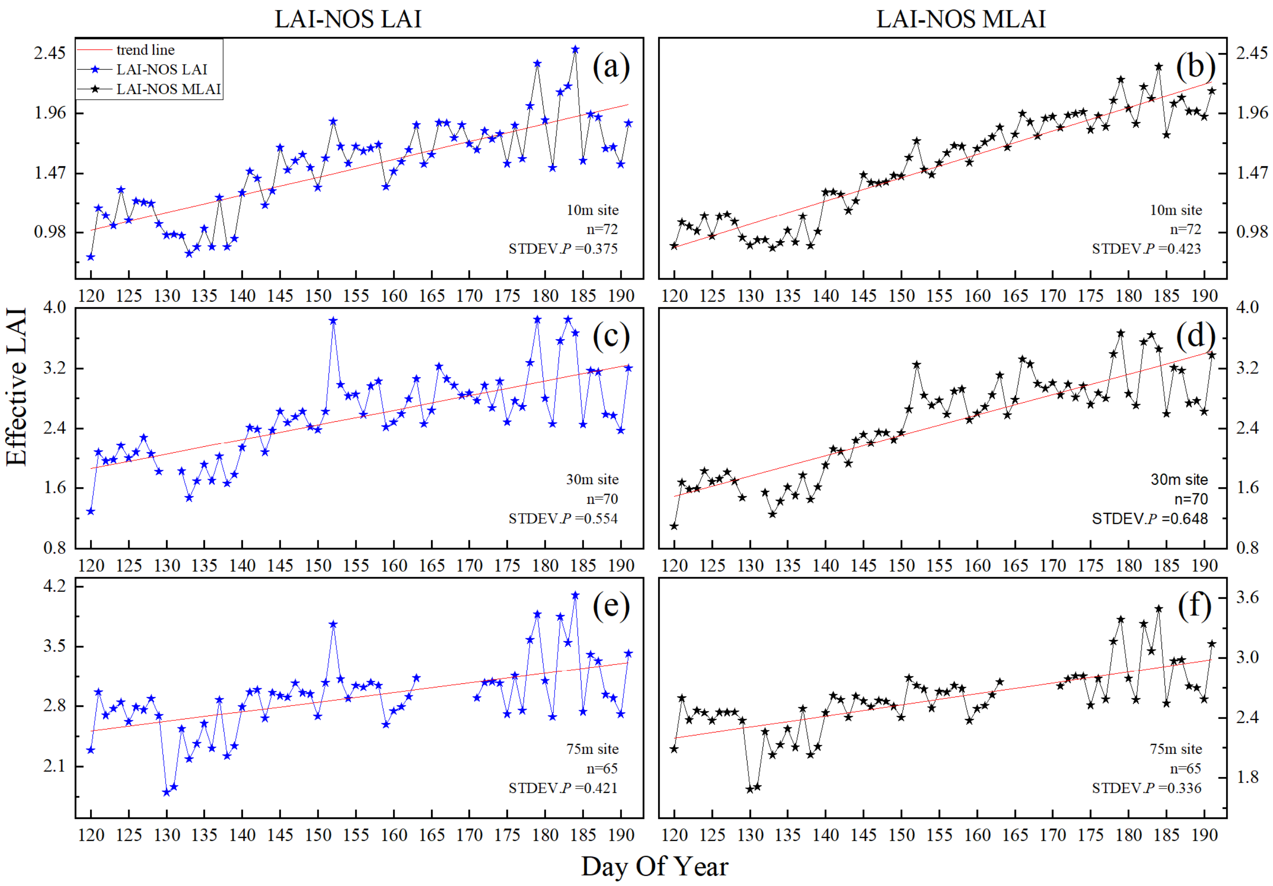

Figure 14. Time series of LAI and MLAI measured by LAI-NOS in three sample sites. (**a**,**c**,**e**) are LAI-NOS LAI time series at 10 m site, 30 m site and 75 m site respectively; (**b**,**d**,**f**) are LAI-NOS MLAI time series at 10 m site, 30 m site and 75 m site respectively.

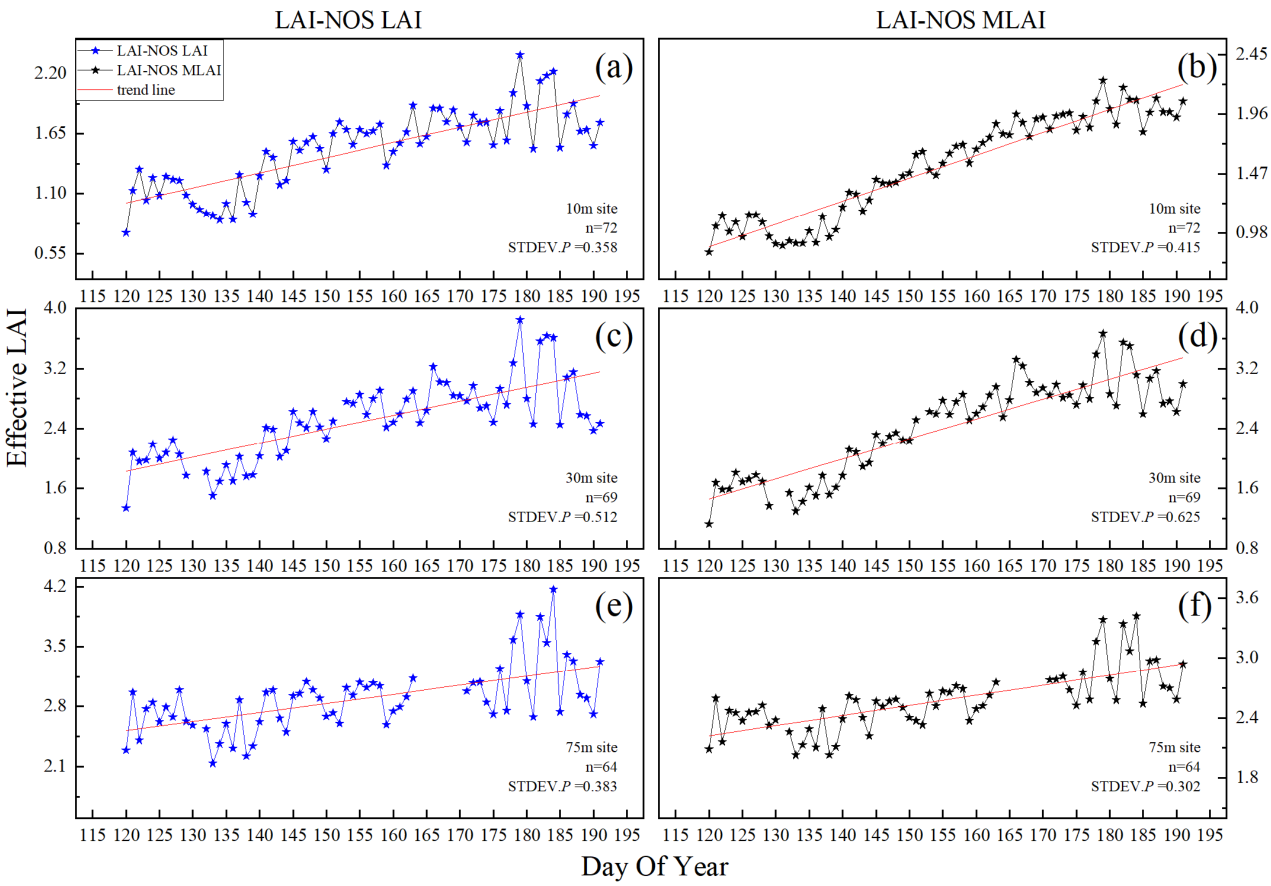

Figure 15. Time series of LAI and MLAI measured by LAI-NOS in three sample sites (CL = 0.8). (**a**,**c**,**e**) are LAI-NOS LAI time series at 10 m site, 30 m site and 75 m site respectively; (**b**,**d**,**f**) are LAI-NOS MLAI time series at 10 m site, 30 m site and 75 m site respectively.

By using a confidence level threshold of 0.8 for data filtering, the LAI values still reflect the same vegetation growth trend. In cases where there were multiple days of precipitation, the confidence level of LAI and MLAI results at the three sites was very low. Therefore, measurements with confidence levels below 0.8 were removed. As shown in Figure 15, the time series data after filtering are smoother and more reasonable, demonstrating that the confidence level parameter provided by the LAI-NOS automatic observation system can help users conveniently and effectively screen the data.

4. Discussion

4.1. Applicability and Accuracy of Manual Measurement Results

As Figure 11, except for the LAI-2200, all instruments exhibit a consistent trend: LAI values are highest at 75 m and lowest at 10 m, aligning with on-site observations. However, the LAI-2200 shows inconsistencies, with the 30 m site having the highest LAI, likely due to complex environmental conditions and measurement timing differences [39].

Complex environmental factors and varying measurement dates, 29 and 30 May, influenced by weather and lighting, contribute to discrepancies. Dense vegetation and challenging terrain affect indirect LAI measurements. The LAI-2200, used in double-probe mode, faces challenges in suitable data collection areas and varying lighting conditions, especially in cloudy weather and mountainous forests, leading to occasional zero measurements.

Consequently, the correlation between LAI-2200 and other methods is low, while consistency is observed between the DHP method and LAI-probe due to shared algorithmic approaches [30]. Figure 12 shows lower determination coefficients and higher root mean square errors for MLAI results compared to LAI results, highlighting significant measurement discrepancies when employing different calculation methods.

4.2. LAI-NOS Daily LAI Data Extraction Method

Previous studies have highlighted the significant influence of lighting conditions on indirect LAI measurements using optical methods, with blue light scattering under direct sunlight causing up to a 20% underestimation of effective LAI [40]. Additionally, changes in shutter speed or aperture can lead to approximately 10% variations in LAI derived from hemispherical photography [41]. To mitigate these effects, instruments are recommended to be used under scattered light conditions, such as before sunrise, after sunset, or on cloudy days. However, conducting experiments only on cloudy days is challenging due to their limited occurrence around sunrise and sunset. Automated instruments offer a solution by enabling continuous 24 h measurements, provided local sunrise and sunset times are considered. In this study, we propose a further optimization called the "sunrise–sunset" method, averaging LAI values measured at these times to obtain daily values. Compared to the "smoothest window" method, the new approach exhibits less variability and a more significant LAI variation trend (see Figure 13).

The study area's mountainous terrain and dense vegetation make canopy lighting conditions complex, posing challenges for accurately extracting daily LAI values using the "smoothest window" method. Conversely, the uniform scattered light before sunrise and after sunset ensures even illumination, facilitating clear canopy images against the sky background and accurate image segmentation. Furthermore, considering potential dew or night rain impacts on the LAI-NOS sensor and the consistency of morning and evening measurements, this study provides confidence levels for calculated daily LAI results to filter out abnormal data caused by exceptional weather conditions.

In Figure 16, morning and evening thumbnails from the 75 m site show significant snow cover that melt throughout the day. Filtering out unreliable measurements with confidence levels of 0.33 and 0.43 ensures data accuracy. Post-filtering, LAI data exhibits reduced variability and a clear upward trend, reflecting vegetation growth (see Figure 13).

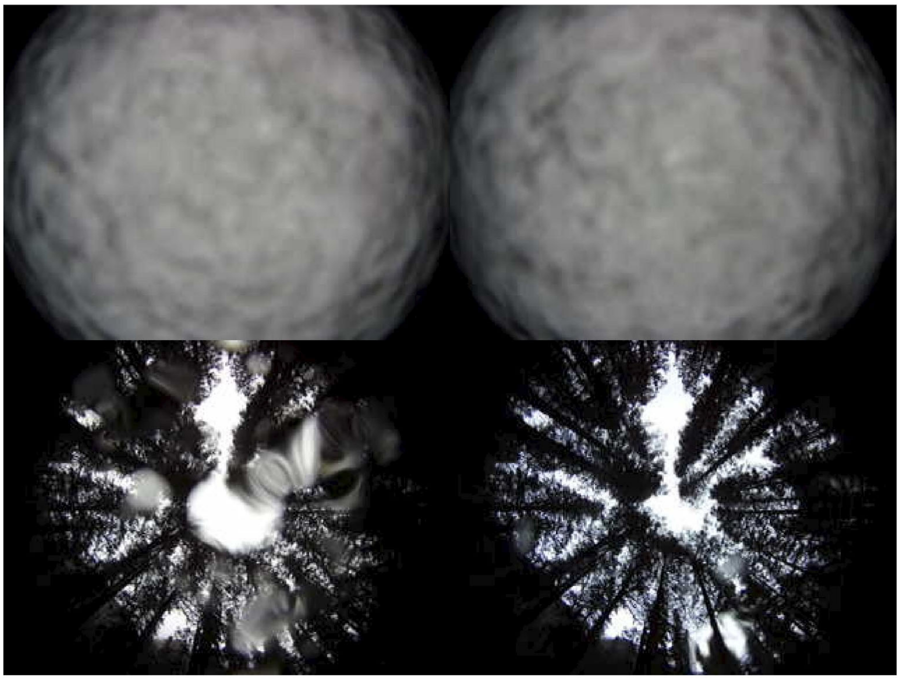

Figure 16. Thumbnails of LAI-NOS returned on the day of low confidence.

Early experiment fluctuations (Figure 10) likely stem from manual adjustments post-LAI-NOS node installation. The LAI data offers agricultural applications beyond forest monitoring, aiding crop yield prediction, ecological management, and fertilizer determination [7,42]. Adaptable LAI-NOS mounts can suit specific crop observations, potentially requiring height reduction or downward sensor arrangement for low crops, with image segmentation adjustments for accurate delineation against varied backgrounds.

4.3. Multi-Angle Method and Single-Angle Method

From Figure 10, it can be observed that, except for the 10 m sampling site, the Multi-angle LAI (MLAI) data show higher correlation between adjacent two days compared to the LAI data (as indicated by the higher number of data points within the red area). This indicates that within the study area, the stability of LAI values calculated using the multi-angle method is superior to those obtained from LAI values.

This improvement in stability may be attributed to the complex lighting conditions within the study area, with many measurement points located on hilly slopes. The multi-angle method allows for increased sampling area, reducing the impact of these factors on the measurements. Consequently, the multi-angle method is better suited for obtaining stable LAI values in such complex terrain and lighting conditions.

4.4. The Influence of Topographic Factors on LAI Measurement

In mountainous terrain, LAI measurements are affected by complex topography, leading to errors when mountains enter the fisheye field of view, as depicted in Figure 3. Surrounding mountains alter the fisheye lens boundary, causing overestimation of LAI and MLAI. Traditional methods like masks or caps may not improve accuracy and could introduce larger deviations.

Future LAI-NOS deployment in such areas requires technical measures to minimize elevated measurements from mountains entering the field of view. Ground LAI measurements in mountains should also consider methods to mitigate mountains' influence on handheld optical instruments.

5. Conclusions

A comparative validation study was conducted on the LAI automatic observation device, LAI-NOS, installed in three sampling sites at Wanglang Mountain Ecological Remote Sensing Integrated Observation Station. Three manual measurement methods (LAI-2200, LAI-probe, and digital camera DHP method) were used to verify the LAI-NOS results. The results showed that LAI-NOS measurements demonstrated good stability and precision and exhibited strong correlations with data obtained from manual measurement instruments, confirming the reliability of LAI-NOS measurements.

The relative errors between adjacent two days for LAI-NOS at the three sampling sites were less than 13% and showed good correlation, verifying its measurement stability. However, the fluctuation amplitude of manual LAI-2200 measurements at the 75 m site did not align with the LAI trends obtained using other methods, indicating its limited applicability in the study area. LAI-NOS results for all three sampling sites were within a reasonable range and demonstrated good correlations with data obtained from manual instruments, validating the accuracy of LAI-NOS measurements.

The manual measurement results contained several obvious outliers, suggesting that the accuracy of manual measurement methods was relatively low in the study area and required careful screening before use. LAI-2200 measurements contained multiple invalid values, indicating limitations in measuring mountainous forest LAI.

The "sunrise–sunset" method, based on the average LAI measurement at sunrise and sunset, demonstrated higher scientific validity compared to the "smoothest window" method. It not only effectively reflected the vegetation growth trend but also showed lower variability in LAI measurements, which is beneficial for capturing vegetation phenological changes. Additionally, this study introduced the concept of confidence in automatic LAI measurement, reflecting the influence of weather conditions on LAI values. Through confidence-based LAI value screening, uncertainty caused by rainy or snowy weather was effectively avoided, which is crucial for outdoor automatic measurement instruments.

Compared to manual instruments, automatic instruments provided significantly improved accuracy by selecting suitable measurement times. Moreover, automatic measurement instruments allowed for continuous observation over long periods, with high temporal frequency, enabling better detection of subtle changes in vegetation phenology due to climate change. This will offer more favorable means for validating remote sensing products and climate change research.

Author Contributions: Conceptualization, Z.G. and Y.C.; methodology, Z.G.; software, Z.G. and T.D.; investigation, Z.G., T.D., J.C. and Z.Z.; formal Analysis, Z.G.; writing—original draft, Z.G.; funding acquisition, Y.C.; supervision, Y.C. and A.L.; writing—review and editing, Y.C.; resources, A.L., Z.Z. and J.C. All authors have read and agreed to the published version of the manuscript.

Funding: This work is supported by the National Key Research and Development Program of China (2020YFA0608702) and the Sichuan Science and Technology Plan Project (No. 2019YJ0201).

Data Availability Statement: Restrictions apply to the availability of these data. Data were obtained from the Wanglang Mountain Ecological Remote Sensing Comprehensive Observation and Experiment Station and are available with the permission of the Wanglang Mountain Ecological Remote Sensing Comprehensive Observation and Experiment Station.

Acknowledgments: We would like to acknowledge the support of the Institute of Mountain Hazards and Environment, Chinese Academy of Sciences. We would like to acknowledge the students in our team on instruments installation and data procession.

Conflicts of Interest: The authors declare no conflicts of interest.

References

1. Chen, J.M.; Black, T.A. Defining Leaf-Area Index for Non-Flat Leaves. *Plant Cell Environ.* **1992**, *15*, 421–429. [CrossRef]
2. Perez, G.; Coma, J.; Chafer, M.; Cabeza, L.F. Seasonal influence of leaf area index (LAI) on the energy performance of a green facade. *Build. Environ.* **2022**, *207*, 18. [CrossRef]
3. Cutini, A.; Matteucci, G.; Mugnozza, G.S. Estimation of leaf area index with the Li-Cor LAI 2000 in deciduous forests. *For. Ecol. Manag* **1998**, *105*, 55–65. [CrossRef]
4. Clark, D.B.; Olivas, P.C.; Oberbauer, S.F.; Clark, D.A.; Ryan, M.G. First direct landscape-scale measurement of tropical rain forest Leaf Area Index, a key driver of global primary productivity. *Ecol. Lett.* **2008**, *11*, 163–172. [CrossRef] [PubMed]
5. Tian, Y.; Zheng, Y.; Zheng, C.M.; Xiao, H.L.; Fan, W.J.; Zou, S.B.; Wu, B.; Yao, Y.Y.; Zhang, A.J.; Liu, J. Exploring scale-dependent ecohydrological responses in a large endorheic river basin through integrated surface water-groundwater modeling. *Water Resour. Res.* **2015**, *51*, 4065–4085. [CrossRef]
6. Iio, A.; Hikosaka, K.; Anten, N.P.R.; Nakagawa, Y.; Ito, A. Global dependence of field-observed leaf area index in woody species on climate: A systematic review. *Glob. Ecol. Biogeogr.* **2014**, *23*, 274–285. [CrossRef]
7. Taugourdeau, S.; le Maire, G.; Avelino, J.; Jones, J.R.; Ramirez, L.G.; Quesada, M.J.; Charbonnier, F.; Gomez-Delgado, F.; Harmand, J.M.; Rapidel, B.; et al. Leaf area index as an indicator of ecosystem services and management practices: An application for coffee agroforestry. *Agric. Ecosyst. Environ.* **2014**, *192*, 19–37. [CrossRef]
8. Tsialtas, J.T.; Baxevanos, D.; Maslaris, N. Chlorophyll Meter Readings, Leaf Area Index, and Their Stability as Assessments of Yield and Quality in Sugar Beet Cultivars Grown in Two Contrasting Environments. *Crop Sci.* **2014**, *54*, 265–273. [CrossRef]
9. Fang, H.; Baret, F.; Plummer, S.; Schaepman-Strub, G. An overview of global leaf area index (LAI): Methods, products, validation, and applications. *Rev. Geophys.* **2019**, *57*, 739–799. [CrossRef]
10. Wang, Y.; Woodcock, C.E.; Buermann, W.; Stenberg, P.; Voipio, P.; Smolander, H.; Häme, T.; Tian, Y.; Hu, J.; Knyazikhin, Y.; et al. Evaluation of the MODIS LAI algorithm at a coniferous forest site in Finland. *Remote Sens. Environ.* **2004**, *91*, 114–127. [CrossRef]
11. Hill, M.J.; Senarath, U.; Lee, A.; Zeppel, M.; Nightingale, J.M.; Williams, R.D.J.; McVicar, T.R. Assessment of the MODIS LAI product for Australian ecosystems. *Remote Sens. Environ.* **2006**, *101*, 495–518. [CrossRef]
12. Chen, Y.P.; Jiao, S.F.; Cheng, Y.L.; Wei, H.C.; Sun, L.; Sun, Y. LAI-NOS: An automatic network observation system for leaf area index based on hemispherical photography. *Agric. For. Meteorol.* **2022**, *322*, 108999. [CrossRef]
13. Fang, H.L.; Wei, S.S.; Liang, S.L. Validation of MODIS and CYCLOPES LAI products using global field measurement data. *Remote Sens. Environ.* **2012**, *119*, 43–54. [CrossRef]
14. Jonckheere, I.; Fleck, S.; Nackaerts, K.; Muys, B.; Coppin, P.; Weiss, M.; Baret, F. Review of methods for in situ leaf area index determination-Part I. Theories, sensors and hemispherical photography. *Agric. For. Meteorol.* **2004**, *121*, 19–35. [CrossRef]
15. Weiss, M.; Baret, F.; Smith, G.J.; Jonckheere, I.; Coppin, P. Review of methods for in situ leaf area index (LAI) determination Part II. Estimation of LAI, errors and sampling. *Agric. For. Meteorol.* **2004**, *121*, 37–53. [CrossRef]

16. Fang, H.L.; Li, W.J.; Wei, S.S.; Jiang, C.Y. Seasonal variation of leaf area index (LAI) over paddy rice fields in NE China: Intercomparison of destructive sampling, LAI-2200, digital hemispherical photography (DHP), and AccuPAR methods. *Agric. For. Meteorol.* **2014**, *198–199*, 126–141. [CrossRef]
17. Garriques, S.; Shabanov, N.V.; Swanson, K.; Morisette, J.T.; Baret, F.; Myneni, R.B. Intercomparison and sensitivity analysis of Leaf Area Index retrievals from LAI-2000, AccuPAR, and digital hemispherical photography over croplands. *Agric. For. Meteorol.* **2008**, *148*, 1193–1209. [CrossRef]
18. Fang, H.L.; Ye, Y.C.; Liu, W.W.; Wei, S.S.; Ma, L. Continuous estimation of canopy leaf area index (LAI) and clumping index over broadleaf crop fields: An investigation of the PASTIS-57 instrument and smartphone applications. *Agric. For. Meteorol.* **2018**, *253*, 48–61. [CrossRef]
19. Morsdorf, F.; Kotz, B.; Meier, E.; Itten, K.I.; Allgower, B. Estimation of LAI and fractional cover from small footprint airborne laser scanning data based on gap fraction. *Remote Sens. Environ.* **2006**, *104*, 50–61. [CrossRef]
20. Qu, Y.H.; Wang, Z.X.; Shang, J.L.; Liu, J.G.; Zou, J. Estimation of leaf area index using inclined smartphone camera. *Comput. Electron. Agric.* **2021**, *191*, 106514. [CrossRef]
21. Zhang, Y.Q.; Chen, J.M.; Miller, J.R. Determining digital hemispherical photograph exposure for leaf area index estimation. *Agric. For. Meteorol.* **2005**, *133*, 166–181. [CrossRef]
22. Yang, R.J.; Liu, L.; Liu, Q.; Li, X.H.; Yin, L.Z.Y.; Hao, X.J.; Ma, Y.S.; Song, Q. Validation of leaf area index measurement system based on wireless sensor network. *Sci. Rep.* **2022**, *12*, 4668. [CrossRef] [PubMed]
23. Qu, Y.H.; Han, W.C.; Fu, L.Z.; Li, C.R.; Song, J.L.; Zhou, H.M.; Bo, Y.C.; Wang, J.D. LAINet—A wireless sensor network for coniferous forest leaf area index measurement: Design, algorithm and validation. *Comput. Electron. Agric.* **2014**, *108*, 200–208. [CrossRef]
24. Comella, L.M.; Goldschmidtboeing, F.; Kluppel, J.; Hager, E.; Woias, P. An innovative sensor for the simultaneous measurement of Photosynthetic Active Radiation (PAR) and Leaf Area Index (LAI). In Proceedings of the 2022 IEEE Sensors, Dallas, TX, USA, 30 October–2 November 2022; pp. 1–4.
25. Kim, J.; Ryu, Y.; Jiang, C.; Hwang, Y. Continuous observation of vegetation canopy dynamics using an integrated low-cost, near-surface remote sensing system. *Agric. For. Meteorol.* **2019**, *264*, 164–177. [CrossRef]
26. Culvenor, D.S.; Newnham, G.J.; Mellor, A.; Sims, N.C.; Haywood, A. Automated in-situ laser scanner for monitoring forest leaf area index. *Sensors* **2014**, *14*, 14994–15008. [CrossRef] [PubMed]
27. Wen, Y.; Zhuang, L.; Wang, H.; Hu, T.; Fan, W. An Automated Hemispherical Scanner for Monitoring the Leaf Area Index of Forest Canopies. *Forests* **2022**, *13*, 1355. [CrossRef]
28. Park, S.J. Generality and specificity of landforms of the Korean peninsula, and its sustainability. *J. Korean Geogr. Soc.* **2014**, *49*, 656–674.
29. Muscarella, R.; Kolyaie, S.; Morton, D.C.; Zimmerman, J.K.; Uriarte, M. Effects of topography on tropical forest structure depend on climate context. *J. Ecol.* **2020**, *108*, 145–159. [CrossRef]
30. Lee, J.; Cha, S.; Lim, J.; Chun, J.; Jang, K. Practical LAI Estimation with DHP Images in Complex Forest Structure with Rugged Terrain. *Forests* **2023**, *14*, 2047. [CrossRef]
31. Chen, J.; Chen, Y.; Liu, Z.; Sun, Y.; Huang, F. Validation of MODIS LAI Product Using Upscaling Sentinel-2 Decameter-Scale LAI and Field Measured LAI. In Proceedings of the IGARSS 2023-2023 IEEE International Geoscience and Remote Sensing Symposium, Pasadena, CA, USA, 16–21 July 2023; pp. 5119–5122.
32. Liu, C.W.; Kang, S.Z.; Li, F.S.; Li, S.; Du, T.S. Canopy leaf area index for apple tree using hemispherical photography in arid region. *Sci. Hortic.* **2013**, *164*, 610–615. [CrossRef]
33. Zou, J.; Yan, G.; Zhu, L.; Zhang, W. Woody-to-total area ratio determination with a multispectral canopy imager. *Tree Physiol.* **2009**, *29*, 1069–1080. [CrossRef]
34. Li, W.; Fang, H.; Wei, S.; Weiss, M.; Baret, F. Critical analysis of methods to estimate the fraction of absorbed or intercepted photosynthetically active radiation from ground measurements: Application to rice crops. *Agric. For. Meteorol.* **2021**, *297*, 108273. [CrossRef]
35. Liu, J.G.; Pattey, E.; Admiral, S. Assessment of in situ crop LAI measurement using unidirectional view digital photography. *Agric. For. Meteorol.* **2013**, *169*, 25–34. [CrossRef]
36. Chen, Y.P.; Yuan, Z.W.; Ma, C.S.; Dai, X.C.; Wei, H.C.; Chen, Y. Design of Portable Measuring Instrument for Leaf Area Index Based on Hemispheric Photography. *Res. Explor. Lab.* **2020**, *39*, 73–76, (In Chinese with English Abstract).
37. Moghimi, A.; Tavakoli Darestani, A.; Mostofi, N.; Fathi, M.; Amani, M. Improving forest above-ground biomass estimation using genetic-based feature selection from Sentinel-1 and Sentinel-2 data (case study of the Noor forest area in Iran). *Kuwait J. Sci.* **2024**, *51*, 100159. [CrossRef]
38. Stewart, J.A.; Chadwick, V.S.; Murray, A. Investigations into the influence of host genetics on the predominant eubacteria in the faecal microflora of children. *J. Med. Microbiol.* **2005**, *54*, 1239–1242. [CrossRef] [PubMed]
39. Pearse, G.D.; Watt, M.S.; Morgenroth, J. Comparison of optical LAI measurements under diffuse and clear skies after correcting for scattered radiation. *Agric. For. Meteorol.* **2016**, *221*, 61–70. [CrossRef]
40. Leblanc, S.G.; Chen, J.M. A practical scheme for correcting multiple scattering effects on optical LAI measurements. *Agric. For. Meteorol.* **2001**, *110*, 125–139. [CrossRef]

41. Macfarlane, C.; Ryu, Y.; Ogden, G.N.; Sonnentag, O. Digital canopy photography: Exposed and in the raw. *Agric. For. Meteorol.* **2014**, *197*, 244–253. [CrossRef]
42. Amanullah, M.J.H.; Nawab, K.; Ali, A. Response of specific leaf area (SLA), leaf area index (LAI) and leaf area ratio (LAR) of maize (*Zea mays* L.) to plant density, rate and timing of nitrogen application. *World Appl. Sci. J.* **2007**, *2*, 235–243.